

PAPER

Neutral beam prompt loss in LTX- β

To cite this article: W. Capecchi *et al* 2021 *Nucl. Fusion* **61** 126014

View the [article online](#) for updates and enhancements.

You may also like

- [Fusion applications for lithium: wall conditioning in magnetic confinement devices](#)
Robert Kaita
- [Oxidation of lithium plasma facing components and its effect on plasma performance in the lithium tokamak experiment-](#)
A Maan, D P Boyle, R Kaita et al.
- [VUV/XUV measurements of impurity emission in plasmas with liquid lithium surfaces on LTX](#)
Kevin Tritz, Ronald E Bell, Peter Beiersdorfer et al.

Neutral beam prompt loss in LTX- β

W. Capecchi^{1,*}, J.K. Anderson¹, D.P. Boyle², P.E. Hughes²,
A. Maan², R. Majeski², D.B. Elliott³ and C. Hansen⁴

¹ Department of Physics, University of Wisconsin, Madison, WI, United States of America

² Princeton Plasma Physics Laboratory, Princeton, NJ, United States of America

³ Oak Ridge National Laboratory, Oak Ridge, TN, United States of America

⁴ Department of Aeronautics & Astronautics, University of Washington, Seattle, WA, United States of America

E-mail: capecchi@wisc.edu

Received 17 July 2021, revised 10 September 2021

Accepted for publication 30 September 2021

Published 22 October 2021



CrossMark

Abstract

Prompt loss of beam injected fast ions approaches 100% in lithium tokamak experiment-beta (LTX- β) discharges, though significantly improved confinement is expected for the higher current plasmas made available by a recent upgrade to the Ohmic heating power supply. Modeling of fast ions using TRANSP/NUBEAM finds a maximum coupled beam fraction of 76% at the near-term limits of the LTX- β operating space. The full ion orbit code POET is employed to validate NUBEAM results against possible non-adiabatic effects on fast ion orbits, but corrections to the prompt loss fraction due to collisionless transport are found to be small. The graphical method code CONBEAM is used to investigate the topology of fast ion phase space as it relates to neutral beam deposition, and counter-injected NBI is considered as a way to access a region of high field side beam deposition. A metric is developed within the CONBEAM using a beam filament model to estimate the prompt loss fraction and shown to agree well with both POET and NUBEAM, enabling near real-time analysis and potential feedback to operators between plasma discharges.

Keywords: neutral beam injection, lithium tokamak experiment-beta, prompt loss, non-adiabaticity, spherical tokamak, tokamak

(Some figures may appear in colour only in the online journal)

1. Introduction

The lithium tokamak experiment-beta (LTX- β) research project is designed to explore the low-recycling regime of fusion plasmas enabled by lithium (Li) coated plasma facing components (PFCs). Low-Z and liquid coatings enable attractive solutions to major challenges to fusion energy production including tolerance of high heat flux and neutron damage [1]. Lithium has long been known to be an attractive first wall candidate, leading to low-recycling boundaries that lead to improved plasma performance [2]. Flat temperature profiles were recently observed in LTX [3]. This temperature-gradient free regime was accessible with a low-recycling boundary of lithium coated PFCs [4, 5].

A 700 kW neutral beam injection (NBI) system (on loan from TAE technologies) now installed on LTX- β is an integral part of the recent upgrade. Good coupling of the beam to the plasma is particularly important; as edge fueling is incompatible with the low-recycling condition, sustainment through core fueling of NBI is essential in LTX- β [6]. Beyond fueling, the heating and momentum injection effects of NBI are important for several reasons. Super-Alfvénic ions in a low-recycling plasma offer an intriguing area of study through their instabilities and effects of losses to the wall. More pressing is that auxiliary heating allows probing of energy scalings in low-recycling plasmas, continuing work done on CDX-U where energy confinement times exceeded the ITER98P(y, 1) ELM y H-mode scaling by a factor of three [7]. Additionally the flow shear introduced by NBI could provide stabilization against density gradient driven modes [8].

* Author to whom any correspondence should be addressed.

Table 1. Geometric parameters of the equilibria studied here.

Equilibrium	δ	κ	R_{mag} (cm)	R_{lcfs} (cm)
100 981 @468 ms	0.28	1.36	41.4	62.6
100 981 @473 ms	0.21	1.25	40.4	59.3
ESC modeled	0.13	1.54	39.4	59.8

Initial NBI operation and concurrent modeling, however, suggest near total prompt loss of beam ions [9]. In this work we consider ‘prompt’ losses to be any ions lost prior to completion of their first drift orbit [10]. While LTX- β has a major radius $R_0 = 0.4$ m and aspect ratio $A = 1.6$ comparable to other spherical tokamaks such as ST40, MAST, and NSTX-U which have employed [11, 12] or modeled [13] successful NBI heating, it operates at $B_0 = 3.4$ kG and substantially lower plasma current than the other devices. The discharges studied here were limited to around 80 kA, but recent upgrades and ongoing shot development are expected to bring the limit nearer to 150 kA. The START spherical tokamak, operating just above the near-term LTX- β range with plasma currents of 200–300 kA and electron densities between 3.5 – $6.5 \times 10^{19} \text{ m}^{-3}$, showed NBI absorption efficiencies of 60% [14].

In this paper, TRANSP/NUBEAM [15, 16] is the primary tool for studying deposition as a function of plasma parameters (n_e , I_p , E_{beam}). Since NUBEAM models particle behavior by following the guiding center drift equations, a full orbit code (POET) is included to investigate effects of finite Larmor radius and non-adiabaticity. The topology of fast ion confinement and loss regions in phase space is determined using CONBEAM [17], a graphical method identifying confined orbits based on conserved constants of motion. A particle is considered lost in both TRANSP and CONBEAM if the guiding center approaches within a Larmor radius of the limiting surface, and in POET if the full ion orbit intersects the limiting surface. Three equilibria were created to investigate neutral beam deposition. Two were created using the PSI-Tri equilibrium code [18] using discharge 100 981 at two time slices, 468 and 473 ms. These represent ‘early’ and ‘late’ in the discharge, and will be referenced throughout the paper by the shot number and timestamp. The third equilibrium was generated with the ESC code in free boundary mode and will simply be referred to as ‘ESC modeled’. With higher ellipticity and much lower triangularity than the others (see table 1), including this equilibrium offers a perspective on the dependence of beam coupling on plasma shaping parameters. These template discharges were scaled to higher plasma current to reach the projected next phase maximum of $I_p = 150$ kA. Thus only the lowest current discharges in these studies represent actual LTX- β plasmas, and refinement of the modeling awaits successful higher current operation.

The remainder of this paper is organized as follows. Section 2 introduces the full ion orbit code POET and presents a picture of the shell deposition of the prompt loss beam ions. TRANSP/NUBEAM modeling illustrates the dependence of beam confinement in LTX- β plasmas on the plasma current, plasma density, and beam energy, and optimized coupling fractions are presented for the equilibrium studied. In section 3

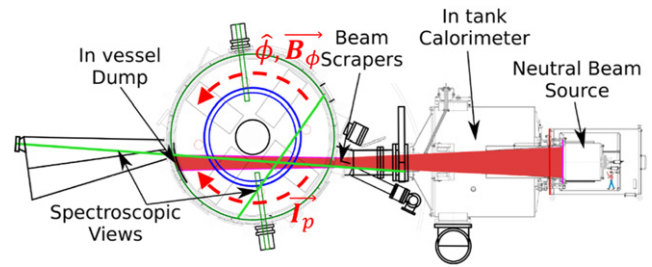


Figure 1. Schematic of the LTX- β vessel and NBI geometry. In normal operation, the beam (shaded red) is co-injected with the plasma current but counter to the toroidal magnetic field.

the conditions necessary for good beam coupling are explored by examining the fast ion topology in LTX- β computed with CONBEAM. Reversed-current operation and altered beam tangency radius may benefit beam coupling. Section 4 gives a discussion of the modeling results and presents comments on non-adiabatic fast ion effects. The development of a CONBEAM metric capable of reporting beam coupling fractions on an inter-shot basis is shown to agree well with NUBEAM and POET calculations. Concluding remarks follow in section 5.

2. Plasma parameters

The journey of a particle (H^0 in the case of the LTX- β NBI) from fuel tank to impact with a material surface is complex. The neutral beam alignment geometry, beam divergence, and beam width determine the trajectories of beam neutrals entering the vessel, after which the location of ionization is determined by the beam energy and local densities and temperatures of the plasma. Figure 1 shows a schematic overhead view of the LTX- β vessel and NBI. The beam path is shown by the shaded red region and travels just over a meter through the vacuum vessel at a tangency radius of 21.3 cm before impacting the beam dump. Once ionized, the particle undergoes one of several possible classes of orbits depending on the magnetic topology. While a great menagerie of orbit types have been documented [19], the equilibria studied here are limited to stagnation and passing trapped orbits, discussed further in section 3. Models of the discharges studied herein show that around 55% of the neutral beam does not ionize in the plasma and simply impacts the beam dump on the far side of the vessel. Of the remaining 45%, nearly all ions drift rapidly upwards, striking the vessel wall before completing a poloidal transit. These ‘prompt loss’ ions exit the plasma within a few microseconds. The impact distribution on the vacuum vessel is highly asymmetric and can lead to large, localized heat fluxes. A POET simulation using a high current equilibrium and high-power beam settings of $E_{\text{nbi}} = 20$ keV and $I_{\text{nbi}} = 35$. A results in a localized peak heat flux of 8 MW m^{-2} (figure 2).

Although the full life of a particle is further complicated by a myriad of other considerations (scattering and slowing down interactions, neutralization, etc) the problem of a well-coupled beam considered within this paper ends with maximizing the fraction of ions deposited onto confined orbits. The fate of a beam neutral within the context of this paper therefore contributes either to the shine-through fraction if it does not ionize

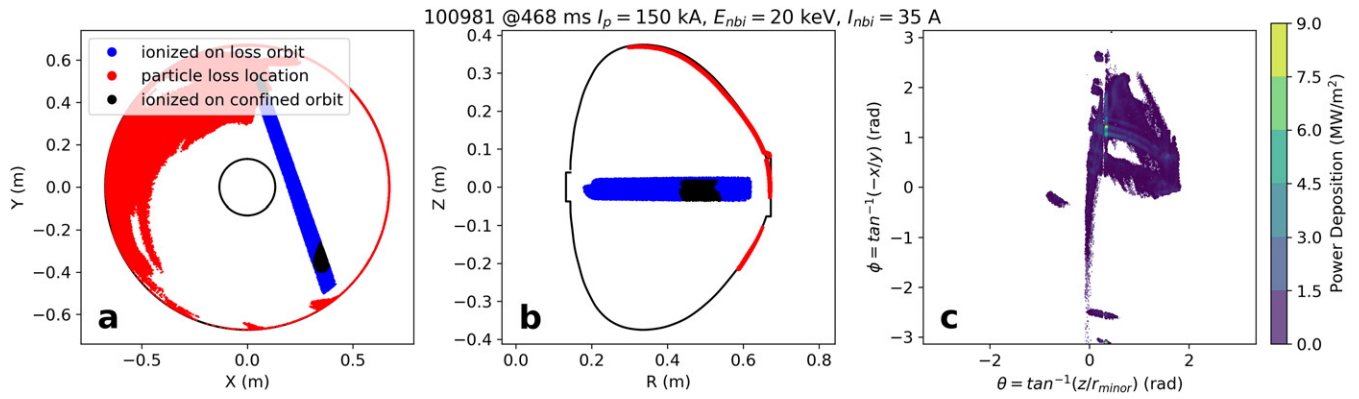


Figure 2. Impact deposition on the shell due to prompt loss of 20 keV, 35 A beam ions. Points of ionization are marked in blue, impact points in red. Black points represent ionization locations that result in confined orbits. The toroidal (a) and poloidal (b) views show the strong asymmetry. The equilibrium studied here resulted in a very localized peak heat flux to the vessel of 8 MW m^{-2} (c).

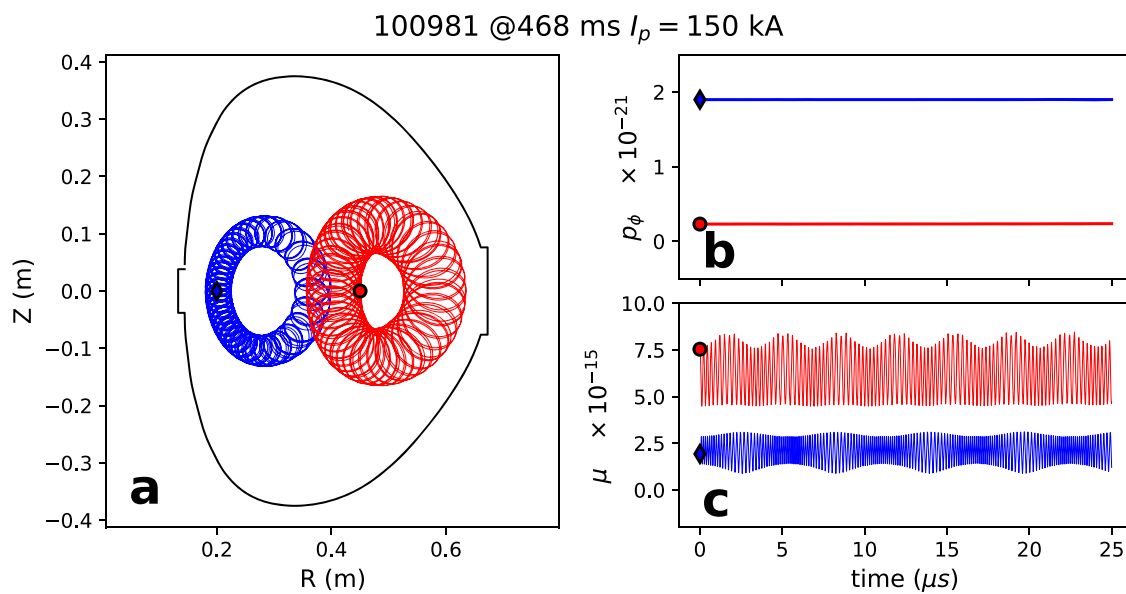


Figure 3. Full orbit examples of a 16 keV beam ion computed with POET. Particle energy (not shown) and canonical angular momentum (b) are well conserved by model. μ is not a constant of the full orbit motion but is conserved over many gyro-orbits (c).

in the plasma, the prompt loss fraction if it is born onto a loss orbit, or the coupled fraction if it is born onto a confined orbit.

The NUBEAM module of TRANSP is a Monte Carlo guiding center code used extensively to model NBI in tokamaks. Due to the relatively large ratio of the fast ion gyroradii to the gradient scale length of the magnetic field in spherical tokamaks however, non-adiabatic effects can be important [20], and for this reason a full ion orbit code, POET, is employed alongside the TRANSP calculations. POET uses a multistep Adams–Bashforth–Moulton method Lorentz solver with an adaptive timestep. Figure 3 shows a pair of well confined orbits calculated with POET in a high current equilibrium. The relative accuracy in the conservation of particle energy and canonical angular momentum is on the order of 10^{-4} or better over the timescales studied here and fast ion orbits were reproduced with a relative accuracy of order 10^{-5} when reversing the direction of time. Similar to NUBEAM, POET uses Monte Carlo methods with information on plasma parameters and

beam geometry to calculate prompt loss fractions and other relevant quantities.

TRANSP modeling allows easy manipulation of plasma parameters, offering a scoping of beam confinement dependence within the present and near term operating limits of LTX- β . To compute the prompt loss fraction, a beam-blip model is used. A $3 \mu\text{s}$ beam pulse imparts a non-perturbative fast ion population to the plasma, and particle tallies are computed $2 \mu\text{s}$ after beam shutoff. This $2 \mu\text{s}$ window is longer than the time required for prompt loss particles to exit the plasma, but short compared to the fast ion slowing down time (8 ms) thus allowing all prompt loss particles to depart while capturing all well-coupled particles before longer timescale effects become important.

Figure 4 illustrates how the shine-through, prompt-loss, and coupled fractions vary with plasma current, plasma density, and beam energy. Both the current and beam energy plots (figures 4(a) and (c)) portray reasonable LTX- β operational

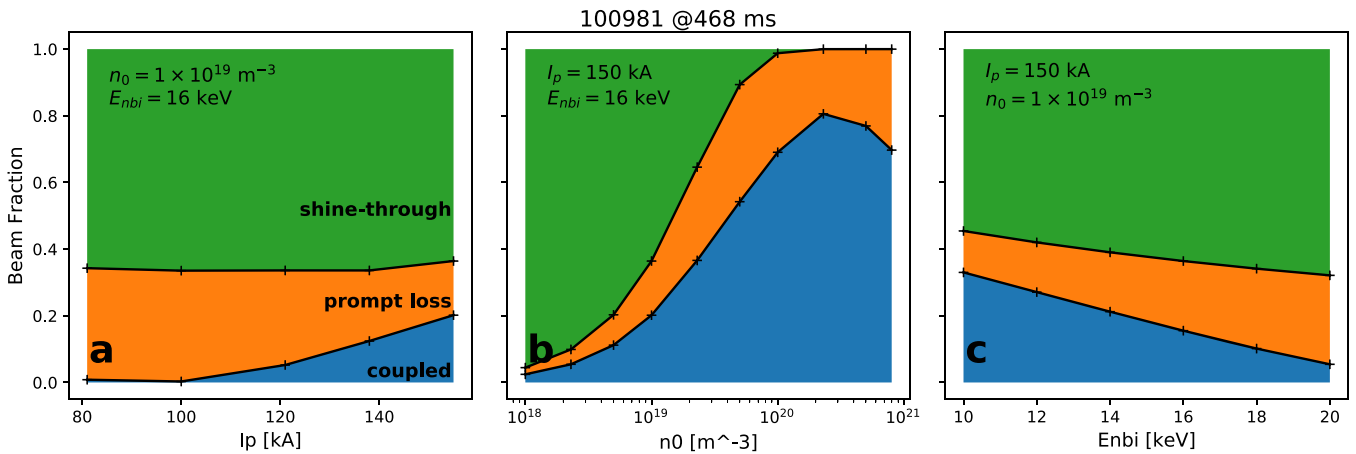


Figure 4. Beam deposition fractions as a function of relevant plasma parameters using TRANSP/NUBEAM. The coupled fraction increases with higher plasma current (*a*), and plasma density (*b*), and with lower beam energy (*c*).

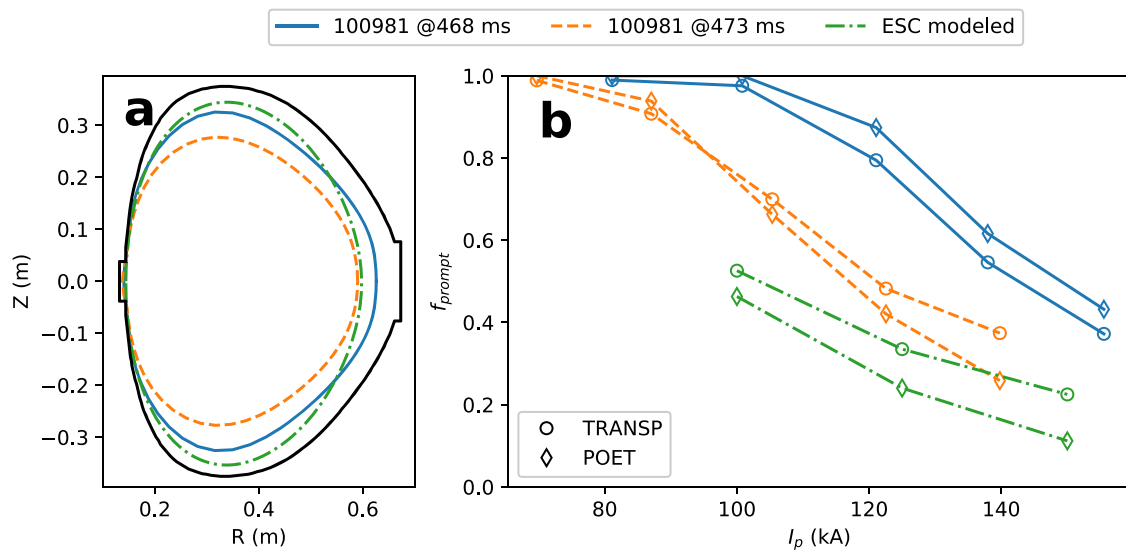


Figure 5. Last closed flux surfaces (*a*) and prompt loss fraction for each equilibrium (*b*), with good agreement between models. Prompt loss diminishes significantly at higher current but variation between the equilibria suggest strong dependence on shaping factors.

ranges, whereas the density scan (figure 4(*b*)) shows higher densities than are achievable to illustrate the inflection point after which the plasma begins to limit beam penetration causing a decrease in confinement. To assess a reasonable upper bound to the beam coupling fraction, a limit of $I_p = 150$ kA is assumed, along with a central plasma density of $n_0 = 5 \times 10^{19} \text{ m}^{-3}$ (line-averaged $n_L \approx 2.4 \times 10^{19} \text{ m}^{-3}$) which is above typical LTX- β densities but below the Greenwald limit of $\sim 7 \times 10^{19} \text{ m}^{-3}$. Using these values, TRANSP predicts a 20 keV beam will result in a coupled fraction of 17%, with shine-through at 15% and the remaining majority, 68% as prompt loss. At 10 keV, the coupled fraction rises significantly to 75%, with shine-through and prompt loss at 5 and 20% respectively. Thus a coupling fraction of 75% is possible within the LTX- β operating range. While a lower energy beam provides better coupling, there are tradeoffs. Notwithstanding other factors such as reduced torque, heating,

or current drive, the NBI provides a source of high energy particles for ChERS impurity temperature measurements. There is a strong dependence on charge exchange cross section with beam energy [21], and in practice a beam energy of 16 keV is necessary to provide sufficient levels of charge exchange to facilitate ChERS measurements. Future NBI operation will therefore likely occur at this energy as a compromise between the competing needs of good beam coupling and sufficient charge exchange signal. At 16 keV, the shine-through, prompt loss, and coupled fractions are 10, 35, and 55%.

Three different equilibrium reconstructions are used to illustrate the sensitivity of beam coupling. The last closed flux surfaces are shown in figure 5(*a*), and the triangularity (δ), ellipticity (κ), major radius of the magnetic axis (R_{mag}), and last closed flux surface (R_{lcf}) are found in table 1. The prompt loss fraction computed by both TRANSP and POET are shown in figure 5 and illustrates, as expected, that beam coupling improves at higher plasma current, but importantly,

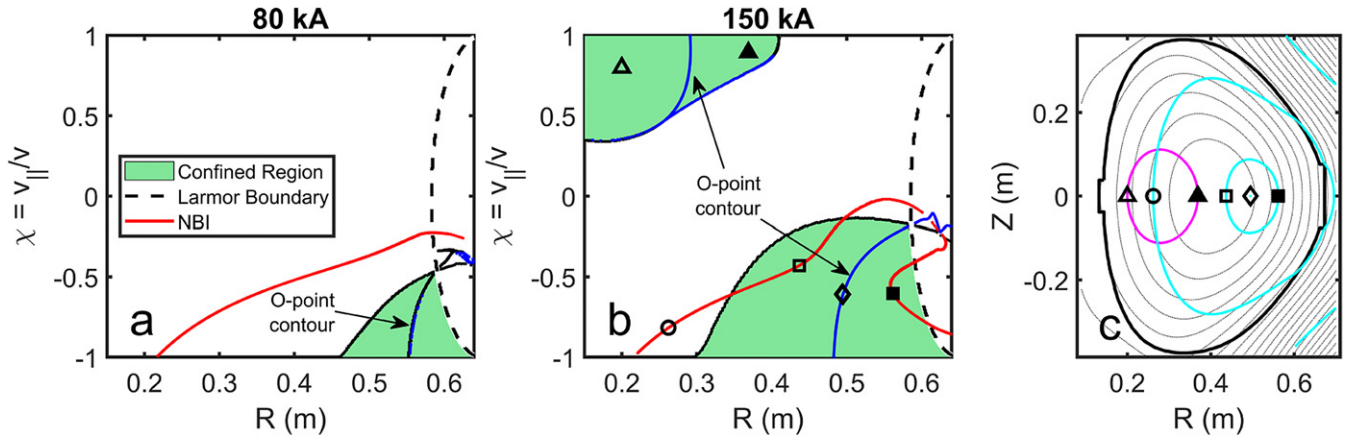


Figure 6. Topological regions in (R, χ) phase space for 16 keV ions in (a) low current (80 kA) and (b) high current (150 kA) equilibrium reconstruction of discharge 100 981 @468 ms. Regions of good confinement (green) are bisected by the O -point contour where guiding center orbit width reduces to zero. Sample orbits marked in (b) are depicted in (c) with the corresponding symbol. For confined orbits, the inner (empty symbol) and outer (filled symbol) orbit leg locations are shown. In (c), cyan lines denote motion in the direction of I_p and magenta lines counter- I_p motion. The orbits denoted by the square and diamond are confined, passing, co- I_p orbits, whereas the triangle marked orbit is a confined, passing, counter- I_p orbit. The orbit with the circle marker is lost.

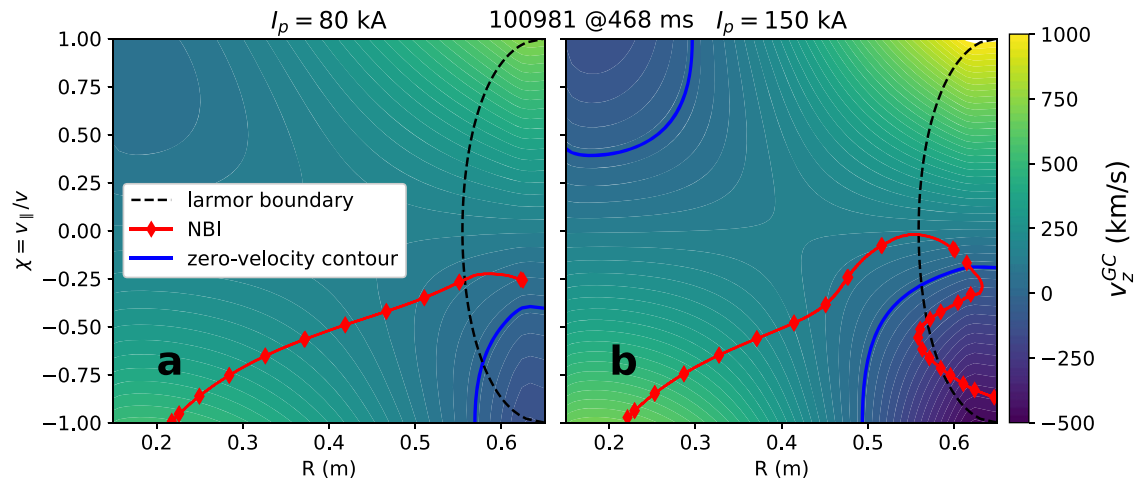


Figure 7. Vertical component of guiding center motion of a 16 keV particle in both a low (a) and high (b) current equilibrium. Orbit legs of the NBI centerline trajectory through phase space are shown in red. The zero-velocity contour (blue) shows close similarity with the O -point contours from figures 6(a) and (b).

that good confinement is achievable for attainable plasma currents. The degree of confinement varies considerably at high current implying that in the transition region between poor and good confinement, beam coupling is quite sensitive to changes in equilibrium parameters and underscores the need for validation of equilibrium parameters when higher current operation becomes available.

3. Fast ion orbit topology in LTX- β

In addition to analyzing optimal plasma operation for maximal beam coupling, it is informative to abstract away from a specific beam injection geometry and consider generally the behavior of fast ions in an LTX- β plasma. The graphical method CONBEAM developed in [17] generates topological boundary maps between different types of ion orbits. CONBEAM assumes both the canonical angular momentum

$p_\phi = q\Psi - Rm v_\parallel B_\phi / B$ and magnetic moment $\mu = m v_\perp / (qB)$ are constants of motion, in which case a complete representation of all potential ion orbits can be cast in terms of the particle's pitch $\chi = v_\parallel / v$ when passing through the midplane at a radial coordinate $S = \pm \sqrt{\Psi}$ where $\Psi = \int_{M.\text{axis}}^{(R,Z)} R |B_\theta \times dl_\theta|$ is the poloidal flux variable integrated from the magnetic axis to points in the (R, Z) plane. Here the midplane is used due to the up-down symmetry of the equilibrium studied, though in general the stagnation surface is used, described in more detail in [17].

In figure 6 the orbit topology of a 16 keV ion is shown. To illustrate the NBI trajectory through this phase space, a simple zero-width (beam filament) model is used. The LTX- β NBI is oriented along the midplane so all along this filament ions are born at $z = 0$ with no vertical component to their velocity. When ionized along the beam filament path, these ions will have a guiding center shifted from the ion position based on

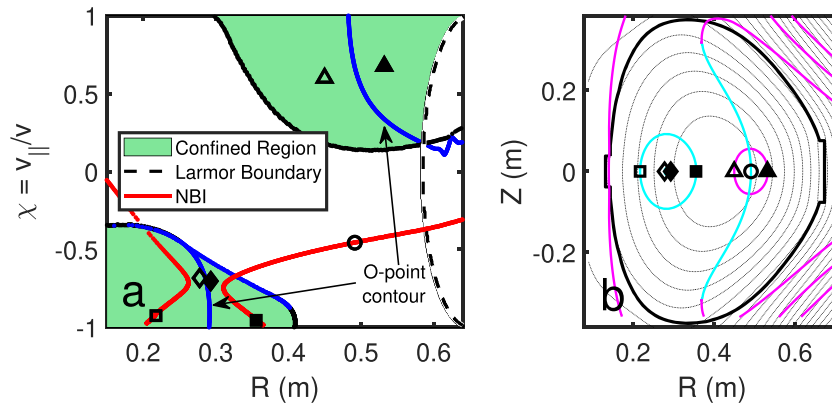


Figure 8. Topology of 16 keV ions in LTX- β for reversed- I_p operation using the high current (150 kA) reconstruction of discharge 100981 @468 ms. The neutral beam trajectory (red) passes through region of good confinement on the high field side. Symbols in (a) correspond to orbits shown in (b). For confined orbits, the inner (empty symbol) and outer (filled symbol) orbit leg locations are shown. In (b), cyan lines denote motion in the direction of I_p and magenta lines counter- I_p motion. The orbits denoted by the square and diamond are confined, passing, co- I_p orbits, whereas the triangle marked orbit is a confined, passing, counter- I_p orbit. The circle marker is on the inner leg of a banana orbit that is lost on the outer leg.

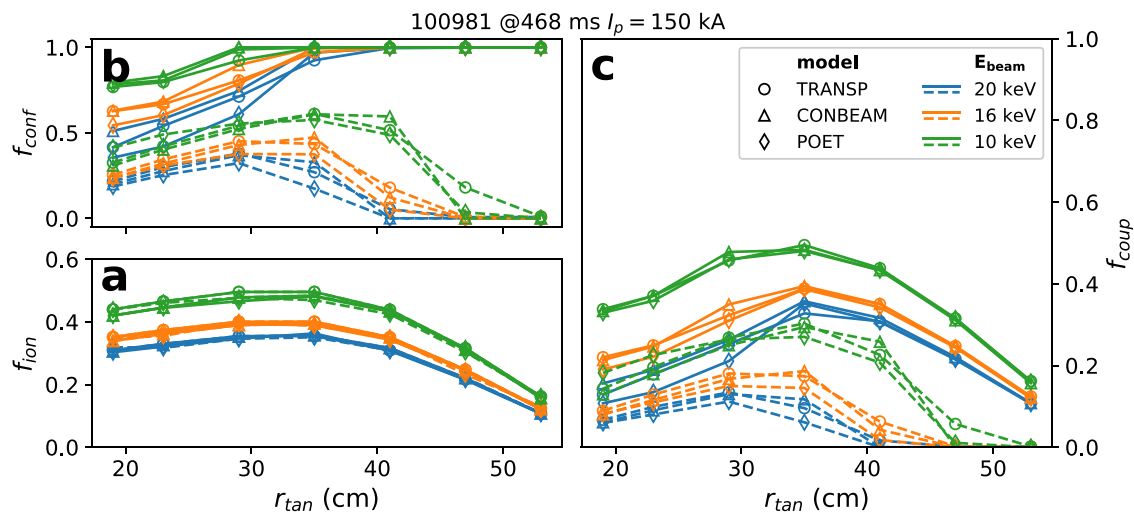


Figure 9. Deposition fractions of the neutral beam vs beam tangency radius (r_{tan}) shows good agreement between TRANSP (circles), CONBEAM (triangles), and POET (diamonds). The projected operating energy of 16 keV (orange) is modeled along with the upper (blue) and lower (green) bounds of the NBI energy range. Both co-(solid) and counter-injection (dashed) cases are shown. (a) The ionization fraction (f_{ion}) falls off at high tangency radius while the confined fraction of the ions (f_{conf}) goes to unity in the co-injected case (b). The resulting coupled fraction (c) of beam neutrals ($f_{coup} = f_{ion}^* f_{conf}$) shows a maximum around $r_{tan} = 35$ cm.

the particle velocity and the local magnetic field, and will be shifted off of the midplane due to the toroidal field component. Because CONBEAM maps phase space at the midplane, the NBI trajectory shown consists of the midplane intersections of the orbits of off-midplane ion guiding center birth locations. Since confined orbits have two midplane intersections (with the exception of orbits along the O -point contour), a pair of traces (such as in figure 6(b)) are observable when the beam filament traverses a region of good confinement. Figure 6 shows that at low current the confinement region is small and does not intersect the NBI trajectory through phase space. The size of the confinement regions increase with I_p , and at the upper range of LTX- β currents the beam generates both confined and lost orbits. The confinement regions in figures 6(a) and (b) are all passing type orbits, characterized by purely positive

or negative pitch (upper left and lower right regions in figure 6(b)). Either increasing the plasma current or decreasing the beam energy improves confinement, which eventually causes the confinement regions to expand across the $\chi = 0$ threshold resulting in confined banana orbits (characterized by orbit legs with oppositely signed pitch). In the case of the equilibrium shown in figure 6(b) this region of confined banana orbits emerges below $E_{nbi} \approx 11$ keV. The Larmor boundary in figures 6(a) and (b) represents the loss region where guiding centers are within a Larmor radius of the limiting surface.

Bisecting each of the confinement regions in figures 6(a) and (b) is the O -point curve where ion orbits reduce to a single point. (See for example the difference in orbit width between the square and diamond marked orbits.) All confined orbits not on this O -point curve are passing particles with an orbit leg

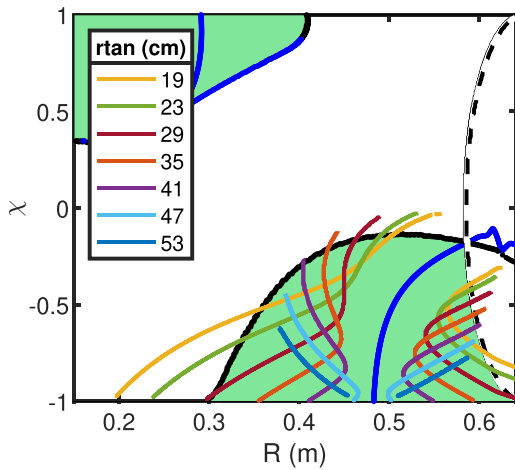


Figure 10. Altering the beam tangency radius influences the beam trajectory through phase space. Larger percentages of the path lengths fall within the confined region for larger tangency radii.

on either side, as depicted by the square and triangle symbols in figures 6(b) and (c). Here positive pitch indicates particles traveling with B_t , and are depicted in magenta in the (R, Z) orbit plots of figures 6(c) and 8(b). The opposite case of negative pitch particles are shown in cyan. Normal operation in LTX- β has the plasma current opposing the direction of the toroidal field (see figure 1) meaning positive pitch indicates motion against I_p . The circle symbol illustrates the loss orbit of a beam neutral that ionizes approaching the beam tangency radius.

The O -point curves in CONBEAM are found by solving

$$\left| \begin{array}{c} \nabla p_\phi \\ \nabla \mu \end{array} \right| = 0, \quad |\nabla p_\phi| |\nabla \mu| \neq 0, \quad (1)$$

where $\nabla = \left(\frac{\delta}{\delta S}, \frac{\delta}{\delta \chi} \right)$ is the gradient of p_ϕ and μ in the (S, χ) phase space. Equation (1) locates the points in (S, χ) space where the gradients of p_ϕ and μ are parallel and non-zero.

A perhaps more intuitive understanding of the origin of this contour can be found by considering the vertical balance between a particle's guiding center and drift velocity. The vertical motion of a particle's guiding center simply the vertical component of the particle's parallel velocity. In an arbitrarily oriented magnetic field this can be written as

$$v_{\parallel z} = \vec{v}_i \cdot \vec{B} \frac{B_z}{B}, \quad (2)$$

where v_i is the ion velocity and \hat{z} the vertical component. The toroidal geometry of a tokamak introduces significant drifts to this motion due to curvature and gradients in the magnetic field so that the initial vertical velocity of the guiding center can be written as

$$v_z^{\text{GC}} = v_{\parallel z} + \frac{K_\perp \vec{B} \times \nabla \vec{B}}{qB B^2} + \frac{2K_\parallel \vec{R}_c \times \vec{B}}{qB R_c^2 B}, \quad (3)$$

where K_\perp, K_\parallel are the particle perpendicular and parallel energies of the particle and R_c the curvature of the magnetic field. This vertical velocity component is shown in the contour plots

in figure 7 as a function of major radius and pitch. The contours of $v_z^{\text{GC}} = 0$ are depicted by the blue lines, and their locations can be understood as follows. LTX- β typically operates with a counter-clockwise ($+\hat{\phi}$) toroidal field and clockwise ($-\hat{\phi}$) plasma current (see figure 1). The direction of the toroidal field results in a ∇B and curvature drift velocity in the $+\hat{z}$ direction over the plasma volume (2nd and 3rd terms on the right of equation (3)). The direction of the plasma current dictates the sign of $v_{\parallel z}$. Particles ionized on the high field side of the magnetic axis are born with a $v_{\parallel z}$ with a sign opposite their pitch (for example a particle with positive pitch will have a $v_{\parallel z} < 0$). The sign is reversed for particles that ionize on the low field side. Since the drift velocity (∇B and curvature) is vertically upward everywhere, the condition $v_z^{\text{GC}} = 0$ can only be met where $v_{\parallel z}$ is negative, i.e. for positive pitch particles on the high field side, or negative pitch particles on the low field side, which is where the zero contours are found in figure 7. Even with such a simple model, the similarity between the zero-velocity contour of figure 7 and the O -point contours of figure 6 is clear.

Also notable in figures 6 and 7 is that for a sufficiently high current, a confinement region appears in the upper left quadrant of (R, χ) space. This region is accessible to the beam if the direction of the plasma current is reversed. Note that reversing the direction of the toroidal field flips both the NBI trajectory and the topological contours resulting in a topologically equivalent injection scenario. (For example, the reversed- B_t versions of figures 6(a) and (b) would be identical, but flipped vertically.) Such a case is shown in figure 8. In the reversed-current scenario the neutral beam trajectory now intersects this region of confined orbits on the high field side of the magnetic axis and provides LTX- β with an entirely new region of deposition to consider for maximal beam coupling.

Because of this tendency to couple *either* on the high or low field side of the plasma, the beam is sub-optimally oriented in this equilibrium. Presently, the beam centerline consists of a roughly 1 m path length through the LTX- β vessel. Of that length, 55% is on the high field side, meaning a large portion of the beam path length is unlikely to couple to the plasma. This percentage is sensitive to the equilibrium studied here and in principle will vary with the location of the magnetic axis. With a tangency radius of 21.3 cm however, it is generally the case that there will always be an appreciable fraction of the beam path length on the high field side. It is therefore important to investigate beam coupling at varied tangency radius with NUBEAM and POET, figure 9. The beam was modeled at both ends of the achievable energy range and for both a clockwise (co-injection) and counter-clockwise (counter-injection) plasma current. The fraction ionized in the plasma (f_{ion}) falls off at higher tangency radius as less of the beam passes through the plasma, but the confined fraction (f_{conf}) of the ionized beam goes to 100% (figures 9(a) and (b)). The total coupled fraction ($f_{\text{coup}} = f_{\text{ion}} \times f_{\text{conf}}$) peaks around $r_{\text{tan}} = 35$ cm as shown in figure 9(c).

In the counter-injection cases shown by the dashed lines, ions are being deposited on the high field side, but as the tangency radius is swept out beyond the magnetic axis, the beam no longer intersects the region of good confinement.

Conversely, in the co-injection cases, the low field side path length increases with tangency radius and the coupled fraction goes to unity though the total coupled fraction is limited by the decreasing ionized fraction. Changing the tangency radius does not only affect the path length, but also alters the phase space deposition, as shown in figure 10, where the higher tangency radius cases push the beam trajectory down into the topological region of good confinement.

A simple estimate of beam coupling fraction can be computed by CONBEAM by using the density and temperature profiles used by TRANSP and POET to compute the transmission fraction along path length of the beam filament through the region of good confinement. These are included in figure 9 and yield a surprisingly good accounting of the beam deposition fractions given the simplicity of the model. For completeness, the beam inclination was also investigated but the existing mid-plane injection was found to be optimal.

4. Discussion

Of the modeling methods mentioned, both TRANSP and CONBEAM, being guiding center codes, assume conservation of the fast ion magnetic moment μ . It has been shown, however, that conservation-breaking occurs, particularly in low aspect ratio devices [20, 22]. The LTX- β NBI produces fast ions with Larmor radii approaching 7 cm resulting in an adiabaticity parameter of $\epsilon = \rho_L/R_a = 0.15$, large enough for non-adiabatic effects to be relevant. CONBEAM has been used to estimate the potential impact of non-adiabatic effects on NSTXp [23]. Variations in μ do not impact p_ϕ , which is conserved under the assumption of toroidal symmetry. Thus particles are still bound to contours of p_ϕ in the orbit topology map. Figure 11 illustrates the reduced confinement region when considering non-adiabatic effects. Ions in the green region will remain confined regardless of the change in magnetic moment. The gray regions represent confined ions susceptible to transitions onto loss orbits due to non-adiabaticity. The degree to which non-adiabatic effects will affect the confined beam population is still being discussed. In [20] it is speculated that non-adiabatic effects may significantly enhance the transport of beam ions, whereas in [23] it is argued that even at infinitely high rates of changes in the magnetic moment the losses of beam ions in NSTX is very limited. Due to the lower operating plasma current in LTX- β , high rates of changes to the magnetic moment would lead to significant loss of the ions in the gray regions in figure 11, significantly impacting the prompt loss fraction.

In [22], however, it is argued that changes in the magnetic moment are small during the slowing down of the beam ions, and only fractional percentage jumps in μ are expected. These jumps occur over a small angular window as the particle crosses the outboard midplane. The poloidal transit period varies depending upon the characteristics of the orbit, but is typically on the order of a few microseconds (for example the modulation in μ observed in figure 3 suggests poloidal transit periods of 3–5 μ s). This implies that confined orbits only transit the small outboard angular window where jumps in μ are expected a few times on a prompt loss timescale, essentially

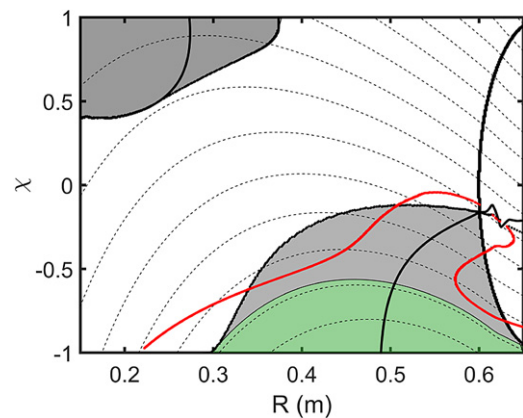


Figure 11. The confined regions (green) are reduced compared to figure 6(b). Regions in gray are confined orbits susceptible to loss due to non-adiabatic effects. These regions are characterized by p_ϕ contours (shown by dashed lines) that intersect a transition boundary or vessel wall.

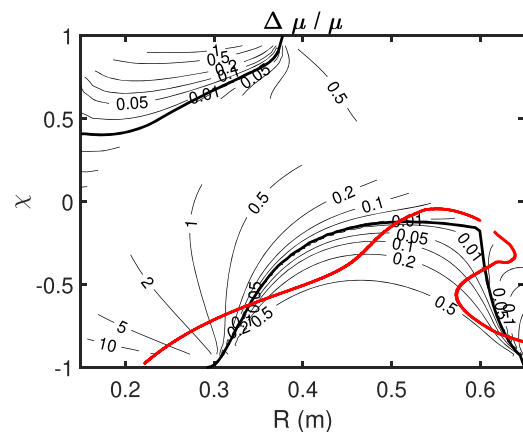


Figure 12. Contours of the fractional change ($\Delta\mu/\mu$) required to move along a contour of p_ϕ to the transition boundary between confined and lost orbits.

demanding a kick in μ sufficiently large to place it immediately on a loss orbit. Figure 12 shows contours of the change in μ required to move to the transition boundary. If ions are limited to only a few fractional percentage jumps in μ on the prompt loss timescale, investigating the beam path traversing the region within 1% of the transition boundary gives a good estimate of the ions in danger of crossing the loss boundary due to non-adiabatic effects. In this equilibrium the total fraction of the beam deposited within the 1% contour of figure 12 is 0.46%, suggesting that non-adiabatic effects on prompt loss is small. It is worth noting that of this 0.46%, 0.26% of the beam is deposited on the loss region side of the transition boundary, meaning these ions are born onto lost orbits but may in fact transition onto confined orbits due to non-adiabatic changes in μ . The remaining 0.2% is born onto confined orbits and may be lost.

Since full ion orbit modeling does not require conservation of the magnetic moment, POET modeling should be sensitive to changes to the prompt loss fraction due to non-adiabatic effects. The similarity between TRANSP and POET

modeling suggests that the influence of non-adiabaticity is small and collisionless transport is unimportant for prompt loss considerations.

The coupled fraction discussed in this work represents the predicted fraction of injected ions born onto confined orbits assuming nominal beam optics. The dependence of the beam optics on the beam current and voltage is being actively researched, and along with the coupled fraction will then enable optimization for fueling current, beam heating, or other quantities of interest. The expectation that beam current scales as $I_{\text{nbi}} \propto E_{\text{nbi}}^{3/2}$ (Child–Langmuir law) suggests that the coupled current ($I_{\text{coup}} = f_{\text{coup}} I_{\text{nbi}} \propto f_{\text{coup}} E_{\text{nbi}}^{3/2}$) will be sensitive to the trade-off between better coupling at lower beam energy, and higher current at higher beam energy.

Non-axisymmetric components of the magnetic fields, arising from eddy currents in the vacuum vessel and first wall components, is important for accurate equilibrium reconstructions on LTX- β [18]. This non-axisymmetry will introduce variations to p_ϕ . Additionally, fast ion losses will lead to the development of an electric potential that may modify both ion and electron confinement. These considerations, however, are beyond the scope of this paper.

A tool capable of measuring fast ion confinement on a routine basis will be useful for optimizing plasma performance for maximal beam coupling, particularly as equilibrium reconstructions have recently been integrated into the LTX- β post-discharge analysis. Such a tool will provide guidance to operators on a shot-to-shot timescale. Both TRANSP and POET are Monte Carlo models making them unsuitable as an inter-shot diagnostic, ruling out the possibility of calculating the prompt loss fraction directly with these codes. With some basic assumptions on the shape of the density profile and electron temperature, estimates of the prompt loss fraction can be computed directly using CONBEAM during the post-discharge analysis. Additionally, equilibria are generated at multiple timesteps for each discharge which will give temporal information on how the confinement fractions are developing during a discharge.

5. Summary

NBI coupling to initial LTX- β plasmas is near zero due to $\sim 50\%$ shine-through and near total prompt loss due primarily to the large vertical drift of the ionized particles. With planned enhancement of the plasma current to 150 kA, a total coupled fraction of 76% will be within the accessible region of parameter space by increasing the plasma density and current and reducing the beam energy. Orbit topology and tangency scan modeling suggest gains are also possible by adjusting the beam injection geometry to a larger tangency radius, though the ultimate value and necessity of such an undertaking should await the refinement of this modeling at higher currents. At sufficiently high current, a region of good confinement appears on the high field side of the magnetic axis which is accessible to the neutral beam when the plasma current direction is reversed and may offer improved coupling fractions for future high current plasmas.

The topology code CONBEAM provides a useful tool for analyzing beam coupling fractions in between discharges and could provide a useful guide to optimize plasma performance for beam coupling.

Acknowledgments

The author would like to thank R. Goldston and L. Zakharov for their discussions and input. This work was supported by DOE Awards DE-SC0019006 and DE-SC0019239.

ORCID iDs

W. Capecchi  <https://orcid.org/0000-0002-0380-0180>
 D.P. Boyle  <https://orcid.org/0000-0001-8091-8169>
 P.E. Hughes  <https://orcid.org/0000-0002-5256-9632>
 A. Maan  <https://orcid.org/0000-0001-7474-2785>
 D.B. Elliott  <https://orcid.org/0000-0003-4535-0381>
 C. Hansen  <https://orcid.org/0000-0001-6928-5815>

References

- [1] Abdou M.A. et al 2001 *Fusion Eng. Des.* **54** 181–247
- [2] Krasheninnikov S.I., Zakharov L.E. and Pereverzev G.V. 2003 *Phys. Plasmas* **10** 1678–82
- [3] Boyle D.P., Majeski R., Schmitt J.C., Hansen C., Kaita R., Kubota S., Lucia M. and Rognlien T.D. 2017 *Phys. Rev. Lett.* **119** 015001
- [4] Schmitt J.C. et al 2013 *J. Nucl. Mater.* **438** S1096
- [5] Maan A. et al 2020 *IEEE Trans. Plasma Sci.* **48** 1463–7
- [6] Elliott D. et al 2020 *IEEE Trans. Plasma Sci.* **48** 1382–7
- [7] Kaita R. et al 2007 *Phys. Plasmas* **14** 056111
- [8] Majeski R. et al 2018 The LTX- β research program and first results *IAEA Fusion Energy Conf.* (Gandhinagar India) (<https://www.iaea.org/events/fec-2018>)
- [9] Hughes P.E. et al 2021 *Plasma Phys. Control. Fusion* **63** 085020
- [10] Heidbrink W.W. and Sadler G.J. 1994 *Nucl. Fusion* **34** 535–615
- [11] Harrison J. 2019 *Nucl. Fusion* **59** 112011
- [12] Menard J.E. 2017 *Nucl. Fusion* **57** 102006
- [13] Salmi A., Gryaznevich M., Buxton P., Nightingale M. and Tala T. 2017 *Fusion Eng. Des.* **117** 14–9
- [14] Akers R.J. et al 2002 *Nucl. Fusion* **42** 122–35
- [15] Goldston R.J., McCune D.C., Towner H.H., Davis S.L., Hawryluk R.J. and Schmidt G.L. 1981 *J. Comput. Phys.* **43** 61–78
- [16] Pankin A., McCune D., Andre R., Bateman G. and Kritiz A. 2004 *Comput. Phys. Commun.* **159** 157–84
- [17] Egedal J. 2000 *Nucl. Fusion* **40** 1597–610
- [18] Hansen C., Boyle D.P., Schmitt J.C. and Majeski R. 2017 *Phys. Plasmas* **24** 042513
- [19] White R.B. 2013 *The Theory of Toroidally Confined Plasmas* 3rd edn (London: Imperial College Press) pp 1–494
- [20] Yavorskij V.A., Darrow D., Goloborod'ko V.Y., Reznik S.N., Holzmüller-Steinacker U., Gorelenkov N. and Schoepf K. 2002 *Nucl. Fusion* **42** 1210–5
- [21] Summers H.P., O'Mullane M.G., Whiteford A.D., Badnell N.R. and Loch S.D. 2007 *AIP Conf. Proc.* **901** 239–48
- [22] Carlsson J. 2001 *Phys. Plasmas* **8** 4725–8
- [23] Egedal J., Redi M.H., Darrow D.S. and Kaye S.M. 2003 *Phys. Plasmas* **10** 2372–81